INVITED PAPER

Goldstone Solar System Radar Observatory: Earth-Based Planetary Mission Support and Unique Science Results

By Martin A. Slade, *Member IEEE*, Lance A. M. Benner, and Arnold Silva

ABSTRACT | The Goldstone Solar System Radar (GSSR) facility is the only fully steerable radar in the world for high-resolution ranging and imaging of planetary and small-body targets. These observations provide information on surface characteristics, orbits, rotations, and polar ices for a wide variety of solar system objects. The resulting data are used not just for scientific studies of these objects, but also for frequent support of the National Aeronautics and Space Administration (NASA) flight projects, including many solar system exploration missions over the last three decades. For example, the GSSR has contributed to the Mars Exploration Rovers (MERs), Cassini, Hayabusa (MUSES-C), MESSENGER, NEAR, SOHO recovery, Mars Pathfinder, Lunar Prospector, Clementine, Magellan, and Viking. Other recent examples include measurement of lunar topography at high resolution near the lunar south pole, which is of particular interest concerning the impact site of the Lunar Crater Observation and Sensing Satellite (LCROSS) mission, and the characterization and orbit refinement of near-Earth asteroids, both for asteroid impact hazard mitigation and for identification of potential targets for future spacecraft missions. We also present important radar scientific results including near-Earth object (NEO) radar imaging of especially interesting objects, and the results from high accuracy determination of Mercury rotation via radar speckle displacement (RSD).

KEYWORDS | Chirp modulation; CW radar; delay estimation; HF radar; planets

I. INTRODUCTION

There are two powerful ground-based radars in the world capable of investigating solar system objects: the National Aeronautics and Space Administration (NASA) Goldstone Solar System Radar (GSSR) and the National Science Foundation (NSF) Arecibo Observatory. NASA derives both scientific and programmatic benefits from their use, including investigations of the Moon, planets, and other solar system bodies, including near-Earth objects (NEOs). These studies provide images and topography, and information on surface characteristics, shapes, composition, orbits, rotations, and distribution of liquids or ices on or below their surfaces. These radars also provide frequent and singular support of NASA missions. The capabilities of these two instruments are different and often provide complementary data, so the combination of results from both radars has often proven to be much more valuable to NASA than each individually, sometimes yielding valuable information that neither could obtain alone. The Arecibo radar is located in Puerto Rico. For a detailed review of the elements of the Arecibo radar, see [1]. This paper will focus on the GSSR.

Manuscript received March 1, 2010; revised August 27, 2010; accepted September 9, 2010. This work was carried out at the Jet Propulsion Laboratory, a division of the California Institute of Technology, under contract with the National Aeronautics and Space Administration (NASA).

M. A. Slade and **L. A. M. Benner** are with the Jet Propulsion Laboratory, California Institute of Technology, Pasadena, CA 91109 USA (e-mail: Martin.A.Slade@jpl.nasa.gov).
A. Silva was with the Jet Propulsion Laboratory, California Institute of Technology, Pasadena, CA 91109 USA. He is now with the Aerospace Corporation, El Segundo, CA 90245 USA.

Digital Object Identifier: 10.1109/JPROC.2010.2081650

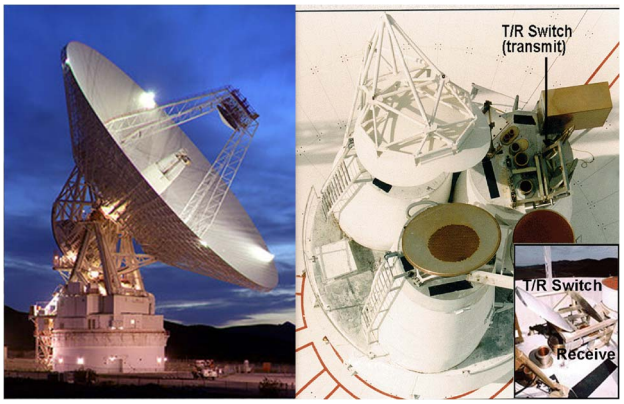

Fig. 1. *(Left) 70-m DSS-14 antenna at the Goldstone DSN complex. Note the three cones below the subreflector on the antenna. (Right) The XKR-cone has the GSSR transmit and receive horns and the transmit/receive (T/R) switch (black arrow). The inset image shows the T/R switch in the receive position.*

II. THE GOLDSTONE RADAR FACILITY DESCRIPTION

A. Overview

The NASA/JPL Deep Space Network (DSN) supports the GSSR. The GSSR consists of a ~500-kW transmitter with center frequency at X-band (8560 MHz or 3.5-cm wavelength) on the 70-m antenna at the Goldstone DSN site (near Barstow, CA). See Fig. 1. GSSR has illuminated targets for reception in multistation mode for receivers at Arecibo Observatory, the very large array (VLA), the very long baseline array (VLBA), Evpatoria (Ukraine), Medicina (Italy), Usuda and Kashima (Japan), as well as five 34-m DSN telescopes also at the Goldstone site. It has performed two-station observations with the 100-m Green Bank Telescope (GBT, Green Bank, WV) for planetary targets Mercury and Venus. (See Appendix I for the locations of the United States telescopes discussed above.)

In the text below, we will introduce the concepts of continuous-wave (CW) radar, radar delay-Doppler mapping, the use of radar interferometry to measure topography, the imaging of NEOs by radar, and various other scientific applications of radar techniques by the GSSR.

B. GSSR Components

The GSSR capability is built around an X-band (8.6 GHz) high-power transmission capability, and can be broken down into the transmitter, receiver, and data-acquisition subsystems. A conceptual diagram of the interfaces and flow among the subsystems is shown in Fig. 2. (A detailed set of actual block diagrams is shown in Appendix II.) The transmitter subsystem consists of two CW Communications Power Industries (CPI) klystrons amplifiers (Fig. 3), along with their associated power system and cooling system. The two Model VKX-7864 250 kW klystrons currently in use are a matched pair that were put in the "X-band-K-band-Research" cone or XKR cone in September 2010. The radar encoding on the transmitted signal is achieved by mixing the signal from an exciter in the transmitter assembly with signals from various waveform generators. The klystrons reside up inside the "XKR cone" on the steerable 70-m antenna, below the subreflector at the prime focus. The high-power radar signal is transmitted out its horn, and a "quasi-optical" transmit–receive (T/R) switch, which is a GSSR component especially developed for NEO applications, allows for receiving with low latency. Because the received signal is acquired through a separate horn connected to a high electron mobility transistor (HEMT)

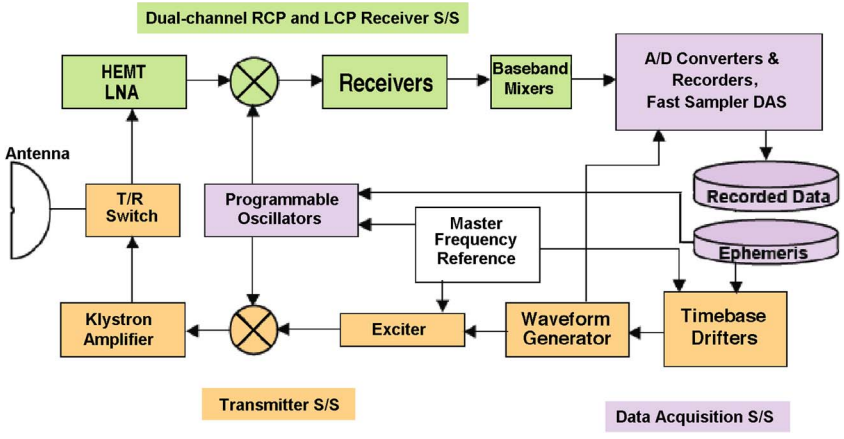

Fig. 2. *Diagram of GSSR subsystem (S/S) interfaces. The dual-channel receiving LNA and data processing chain is capable of recording right-circularly-polarized and left-circularly-polarized (RCP and LCP) signals simultaneously. The T/R switches between the two feed horns, one horn from the transmitter, the other to the LNA. (See Fig. 1.)*

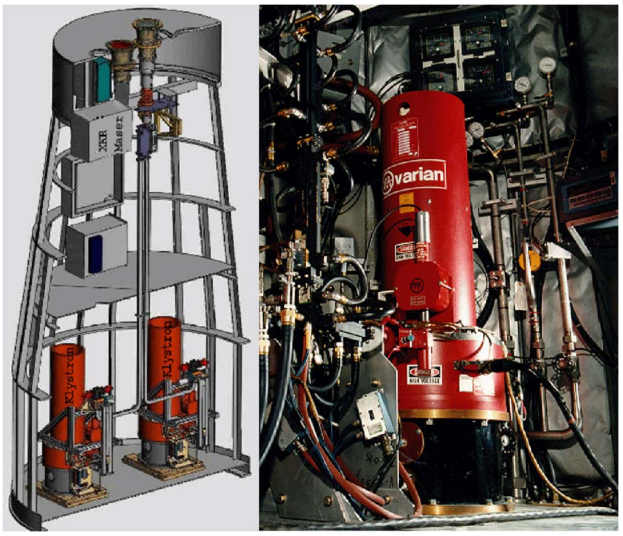

Fig. 3. *GSSR XKR cone and a CPI 250-kW klystron amplifier. The horn leaving the top of the cone in the cone axis is the transmitter horn, and the one to its left is attached to the LNA. (Varian, Inc. merged with several other companies in 2004 to form CPI. The LNA in this figure is labeled "XKR Maser," which has been replaced in 2008 by an X-band high electron mobility transistor or X-HEMT LNA.)*

low noise amplifier (LNA) also located inside the XKR cone, observing nearby NEOs requires switching the transmitter on and off, but also switching between the transmit and receive feeds up on the XKR cone (Fig. 1).

The data acquisition subsystem (DAS) is critical for conversion of the analog signals from the receiver to digital data (A/D converters) that is recorded to disks for offline data analysis. (The receiver performs appropriate signal processing of the LNA's output, depending on the goals of the particular observation.) We include the software that is used to command and control the radar in the DAS. Parts of that software use ephemeris information to drive the programmable oscillators (POs) that are an important part of the GSSR system. The POs take input from the DSN's stable master frequency reference. (See Appendix II for a more complete description of the POs.)

III. RADAR DELAY-DOPPLER MAPPING

The central feature of delay-Doppler mapping is the separation of the backscattered signal from various resolution cells based on their distance (range) and line-of-sight velocity with respect to the observer. The radar observables are the round-trip time delay and Doppler frequency shift, with the Doppler shift arising from orbital and rotational motions of the Earth and the target body. As illustrated in Fig. 4, regions at a given time delay (range) from the radar are planes perpendicular to the line-of-sight direction $\mathbf{i}$. A region with a constant Doppler frequency are planes parallel to a plane containing the line-of-sight direction $\mathbf{i}$ and to the

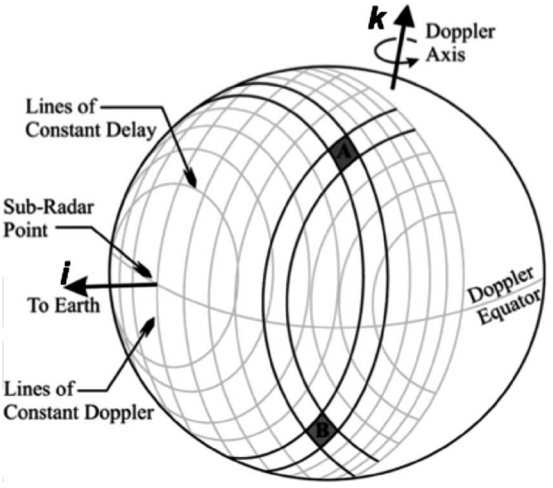

Fig. 4. *Delay-Doppler mapping geometry for a spherical body. Planes of constant time delay from the radar are planes perpendicular to the line-of-sight direction* $\mathbf{i}$*. Planes of constant Doppler frequency are planes parallel to a plane containing the line-of-sight direction* $\mathbf{i}$ *and to the apparent rotation axis* $\mathbf{k}$*. (Figure adapted from [2].)*

apparent rotation axis $\mathbf{k}$. Analyzing the radar echoes in time delay and Doppler frequency thus measures the radar backscatter from different parts of a target.

As shown in Fig. 4, resolution cells on the surface can have the same delay and Doppler values, such that their echo powers combine in a delay-Doppler map (e.g., $\mathbf{A}$ and $\mathbf{B}$ in Fig. 4) and the two physical hemispheres collapse into one. This condition is called the "North–South ambiguity." An example of a delay-Doppler map is shown in Fig. 5 for

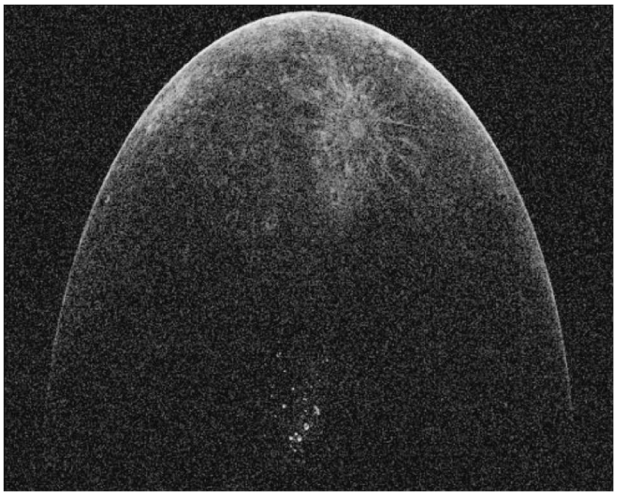

Fig. 5. *Delay-Doppler map of Mercury obtained on June 16, 2000, at Arecibo. The leading edge of the radar echo is the parabolic locus that is brightest at the top. The North Pole craters that are filled with radar-bright material (putatively water ice) are at the bottom center. The delay resolution is 3 km. (From [3].)*

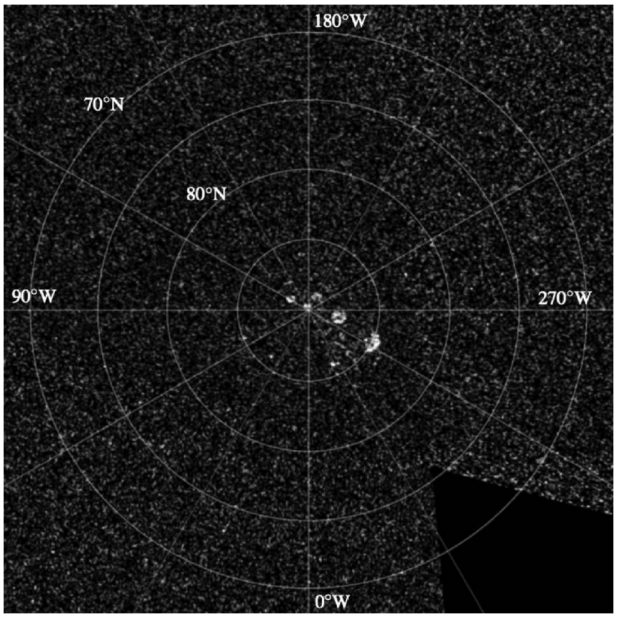

Fig. 6. ***Goldstone image of the North Pole of Mercury obtained in 2001 [4]. The delay-Doppler data were mapped to planetary coordinates in a polar orthographic projection. The resolution is 6 km by 6 km.***

the planet Mercury as seen from Arecibo [3]. The North–South ambiguity is not important here since the terrain to the south of the area imaged is very radar dark. Fig. 6 focuses on the North Polar craters, which are seen at the bottom center of Fig. 5, but imaged with Goldstone data in planetary coordinates from data collected in June and July 2001 [4].

The delay-Doppler technique makes use of the relative motions between imaged area points to create the Doppler resolution. At high spatial resolution, regions at the edges of the imaged area will "smear" due to migration in delay and Doppler cells not accounted for in simple delay-Doppler imagery [5]. Either focused range-Doppler processing or polar-format spotlight-mode processing can be used for better image quality. See discussions of the former method for high-resolution imaging in [5] and the latter method in [6].

IV. RADAR INTERFEROMETRY

Two-station Earth-based radar interferometry can obtain detailed topographic maps of the surfaces of planetary bodies. The technique is similar to terrestrial topographic mapping from interferometric synthetic aperture radar (SAR) observations and was first described in [7] and [8]. Since the original formulation of the technique for lunar mapping, radar interferometry has been applied to terrestrial remote sensing [9]. The technique has been used with considerable success in a variety of geophysical applications [10]. The description here of delay-Doppler mapping and of the basic concept underlying radar interferometry closely follows the approach presented in [7] and [11]. Consider an Earth-based radar system with two receiving stations forming an interferometer. The distance between the two interferometric receiving antennas, *the baseline B*, is assumed to be much smaller than the range R to the target body under consideration. In the usual radar experiment, the experimenter records radar echoes in both amplitude and phase in order to extract information about the material properties and location of the scattering surface. When a radar interferometer is used, additional information about the location of the reflecting surfaces can be obtained because incoming wavefronts have different arrival times at the two receiving antennas. The time delay depends on the orientation of the incident radiation and can be related to the interferometric phase (that is, the phase difference between the two radar echoes). As an example, a 2π phase change is recorded by the interferometer when the orientation of incoming radio waves changes by λ/B_p, where λ is the wavelength and B_p is the baseline projected on the plane perpendicular to the line of sight. At a distance R, this angular difference corresponds to a *fringe spacing* s, which is given by

$$s = R\frac{\lambda}{B_p}. \tag{1}$$

Topographic changes are then related to the measured interferometric phase because the location of reflection elements in the fringe pattern of the interferometer is elevation dependent. Height deviations Δz parallel to the projected baseline produce phase changes $\Delta\phi$ for the interferometer in proportion to

$$\frac{\Delta z}{s} = \frac{\Delta\phi}{2\pi}. \tag{2}$$

Combining (1) and (2), we obtain

$$\Delta z = \frac{R\Delta\phi\lambda}{(2\pi B_p)}. \tag{3}$$

The above basic concepts are used in the topographic mapping for the Moon presented in [12]. See also Section VI.

V. NEAR-EARTH OBJECTS

Ground-based radar is the most powerful astronomical technique for characterizing NEOs and refining their

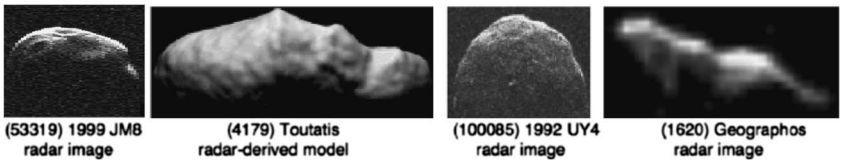

Fig. 7. ***Goldstone NEO images obtained via delay-Doppler mapping ([16]–[19], respectively).***

orbits. While NEOs appear as unresolved points through ground-based optical telescopes, the Arecibo and Goldstone radars can image NEOs with resolution as fine as several meters. Radar has produced the best physical characterizations of potentially hazardous NEOs as large as a kilometer and the best images yet of binary small body systems of NEOs.

Radar echoes from NEOs have revealed both stony and metallic objects, featureless spheroids, and shapes that are elongated and irregular, objects that must be monolithic chunks of solid rock, and objects that must be unconsolidated "rubble piles." See Fig. 7 for examples of delay-Doppler radar images of NEOs. (More elaborate modeling of the shapes of NEOs can be performed using the techniques pioneered by Hudson [13] and more recently updated and documented by Magri [14], [15].)

A. Nonprincipal Axis Rotators

Radar images of 1999 JM8 obtained in 1999 [16] reveal an asymmetric, irregularly shaped, ~7-km-wide object with pronounced topography, prominent kilometer-sized facets, and numerous crater-like features. 1999 JM8 is a nonprincipal axis rotator with a periodicity of order one week.

Delay-Doppler images of the Earth-crossing asteroid 4179 Toutatis achieved resolutions as fine as 125 ns (19 m in range) and 8.3 mHz (0.15 mm/s in radial velocity) and placed hundreds to thousands of pixels on the asteroid, which is 4.5 km long and 2.4 km wide, and heavily cratered [20]. Radar observations from 1992, 1996, and 2004 reveal Toutatis to be in an extremely slow, nonprincipal-axis rotation state with two main periods of 5.4 and 7.3 days. The best shape model has an areal resolution of approximately $(34\ \text{m})^2$ [21].

B. Orbit Refinement

Radar is invaluable for refining the orbits of potentially hazardous NEOs. Range-Doppler shift measurements provide line-of-sight positional astrometry with precision as fine as 4 m in range and 1 mm/s in velocity, with a fractional precision typically 100–1000 times finer than with typical optical measurements [22]. Radar reconnaissance can add decades to centuries for the intervals over which we can predict close Earth approaches and dramatically refines collision probability estimates based on optical astrometry alone, especially for objects passing the Earth for the first time.

The NEO population also provides the most accessible bodies for robotic and human spacecraft missions. Spacecraft operations to these primordial bodies can be greatly aided by radar-derived physical models and precision trajectories of the mission targets, reducing the mission cost, decreasing the complexity in the design of the spacecraft, and improving the odds of a successful mission, be it sample return or hazard mitigation.

C. Binary Asteroid Systems

With binary NEO 1999 KW4, Ostro *et al.* [23] discovered a suite of exotic phenomena, such as a librating secondary, an oblate shape, and a pronounced equatorial ridge rotating at nearly escape velocity (see Fig. 8).

Other multiple-body NEOs observed at Goldstone include contact binary 2007 VD12 in November 2007, and a triple body object 1994 CC first identified as such in June 2009.

D. Higher Range Resolution: Observations in 2010

NEO observations by the GSSR up to 2009 have used only binary phase coded (BPC) waveforms to deliver the range resolution (also known as PN coded) (see, for example, [24]). The best range resolution at Goldstone using BPC waveforms has been limited to 18.75-m resolution (1/8 μs), since any finer resolution violates the frequency license. (GSSR's license from the National Telecommunications and Information Administration (NTIA) is between 8500 and 8620 MHz.)

However, a change in waveform can achieve higher resolution without violating the GSSR license: the linear frequency modulation (LFM or chirp) waveform, which is widely used in synthetic aperture radar (SAR) applications (see, e.g., [25]). (Using a chirp waveform for GSSR ranging is based on an informal report [26].) An internal JPL study [27] found that the practical bandwidth limit for the current Goldstone klystrons is 40 MHz when using chirp waveforms, which leads to an imaging system with 3.75-m resolution—an improvement of a factor of five. (Note that this is twice as fine as the best range resolution of Arecibo's S-band planetary radar.) A sequence of images obtained in January 2010 with 3.75-m range resolution of NEO 2010 AL30 is shown in Fig. 9.

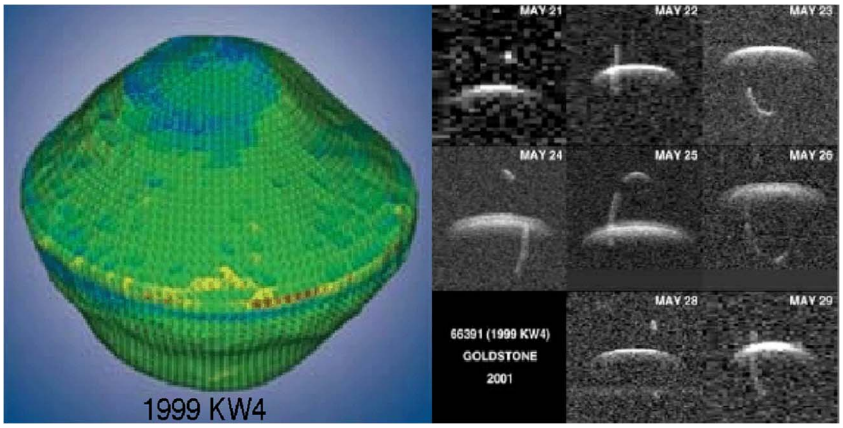

Fig. 8. ***Joint Goldstone/Arecibo radar imaging of asteroid 1999 KW4. Arecibo observations allowed precision modeling of extreme oblateness of primary object (left) while Goldstone observations revealed details of the orbit of secondary object (right) [23].***

By using both a broadband transmitter and a chirp waveform with 150-MHz bandwidth, the range resolution could be as fine as 1 m. With such fine scale imaging, this ground-based radar observatory could produce "spacecraft-encounter-quality" images of NEOs several times per year, providing an extremely low-cost means for NASA to explore a sizable fraction of the NEO population.

VI. THE MOON

NASA is currently planning and performing an ambitious set of lunar robotic missions to determine the topography and gravity field of the Moon to very high precision.

The south pole of the Moon has attracted much recent attention due to the possibility of significant amounts of frozen water being trapped in permanently shadowed regions in craters in that region. Key to understanding of the possibility of the frozen volatiles at the poles of the Moon is detailed knowledge of the lunar polar topography. Radar inteferometry from the Goldstone complex has an ongoing history of providing the most accurate such lunar topographic maps available, with ever-increasing detail revealed as the radar mapping techniques evolve. From topography with 150-m pixels in 1997 [11] for aiding the Lunar Prospector and Clementine Missions to 20-m pixels in 2007, the Goldstone radar was essential. Fig. 10 shows the GSSR imaging of the Lunar North Pole (center) in 2009 compared with two spacecraft images—a composite of the SAR imaging by the Indian lunar orbiter Chandrayan and the optical imaging by the 1994 United States lunar orbiter Clementine—of the same region.

In 2009, the 5-m pixel imaging of the Moon made essential contributions to planning and postimpact analysis for the Lunar Crater Observation and Sensing Satellite

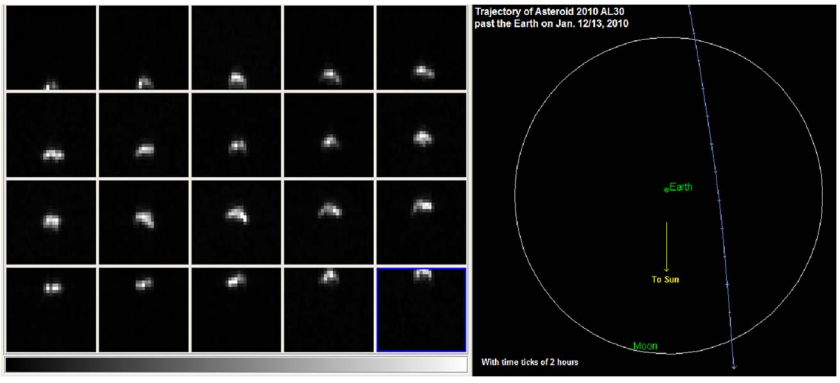

Fig. 9. ***Goldstone delay-Doppler imagery of NEO 2010 AL30 on January 13, 2010, was using the highest resolution chirp waveform. Each frame represents 30 s of integration. Range increases downward; 1.875 m separate each row of pixels. Doppler increases to the right; each pixel column is separated by 0.5 Hz in each frame of the montage. The vertical drift of the echo in the images is due to uncertainties in the ephemeris. The panel on the right shows the trajectory of 2010 AL30 in the vicinity of the Earth and the Moon (orbital image from [28]).***

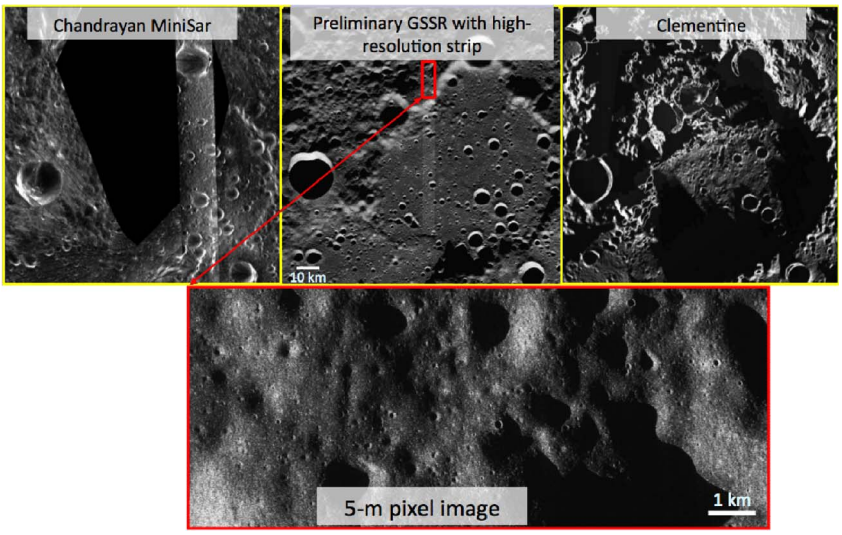

Fig. 10. ***Example of 2009 capability of Goldstone radar at the lunar North Pole compared with two images of the same region from lunar orbiters. The pixel resolution is 5 m by 5 m in the bottom image [12].***

(LCROSS) mission [12]. The Goldstone radar has given good return on investment by timely delivery of high-resolution Lunar maps, with height resolution improving from 50 m in 1997 [11] to 3 m [root mean square (rms)] in 2009–2010.

Even with topographic mapping by a variety of orbiting platforms [e.g., Lunar Reconnaissance Orbiter (LRO)], the topographic maps generated by the Goldstone radar will remain the highest resolution contiguous maps over a large area for the foreseeable future. Although missions such as LRO will generate topographic measurements at points over much of the lunar surface with a vertical accuracy on the order of 1 m, the horizontal separation of these vertical measurements will be less than 20 m only at the poles. At the lunar equator, the horizontal separation will be ~1 km [29]. Optical stereogrammetry-derived digital elevation models (DEMs) will provide high-resolution topographic maps of small selected areas, but lack the large area coverage (10^5 km^2) of a typical Goldstone radar topographic map of portions of the lunar surface.

VII. PLANETARY OBSERVATIONS AND NASA MISSION SUPPORT

Both the Goldstone and Arecibo radars have a long and continuing history of exploring the deeper solar system, both for basic solar system science and for NASA mission support. Present and past uses of these radars are briefly described below, starting with the inner solar system and working outward.

Mercury has long been a target for ground-based radar observations. The Shapiro "fourth" test of general relativity was an early (1964) triumph. Routine radar ranging to Mercury has contributed to knowledge of its orbit for spacecraft to Mercury mission navigation, including Mariner 10 and the current MESSENGER mission. The Goldstone radar is contributing to the MESSENGER mission by precisely measuring the forced longitude librations of Mercury. The technique of observation has been dubbed "radar speckle displacement" effect (RSD effect). In brief, a CW radar reflection from the solid surface of Mercury exhibits spatial irregularities in its wavefront caused by the constructive and destructive interference of waves scattered by the irregular surface of Mercury. The corrugations in the wavefront, also called speckles, are tied to the rotation of Mercury, and will sometimes sweep over the Earth's surface as Mercury rotates. When the trajectory of the speckles is parallel to the baseline between two antennas, the radio signals at the two receiving telescopes show a high degree of correlation after allowing for the time lag from the finite speed of the speckle motion. (Fortunately, the relative locations of the Earth and Mercury and the orientation of their rotation poles are known well enough that it is possible to predict the dates and times of speckle trajectories traversing the baseline of the antennas.) The amount of lag delay that maximizes the correlation of the echoes at the two receiving telescopes can be shown [30] to be directly related to the magnitude and orientation of the spin vector of the planet. The large measured libration amplitudes (see Fig. 11) from Goldstone and the GBT observations (larger than if the entire planet responded to the solar torque) demonstrated that the Mercury mantle must be decoupled from the deeper interior by a molten layer. The pole orientation of Mercury is also being determined with unprecedented accuracy from the same set of radar observations (the discussion above is based on [31] and the references therein).

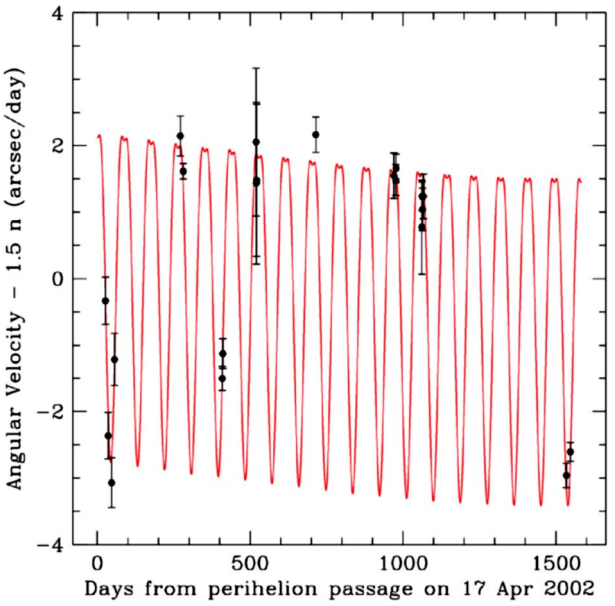

Fig. 11. ***Mercury spin rate deviations from the resonant rate of 3/2 times the mean orbital frequency. Observed data points and their error bars are shown in black. The red line shows a numerical integration of the Sun's torque on Mercury, which is fitted to the data. This fit estimates three parameters, which in effect include the 88-day forced libration and a 12-year free libration. (Figure from [31].)***

The "RSD" technique is also being applied by Margot *et al.* to Venus using Goldstone and the GBT to determine the interaction of the Venus surface with the very dense atmosphere, as well as refinement of the spin rate and pole direction.

Both the Goldstone and Arecibo radars mapped portions of Venus prior to the Magellan mission to determine the Venusian spin rate and pole direction, which allowed the Magellan to enter an optimal mapping orbit around Venus. Both radar observatories determined these quantities from different sets of features on the Venus surface. (See [32] and [33].) The separate determinations agreed very well, and a combination of all the time histories of the Venus radar features led to a choice for the Magellan orbit that worked perfectly.

Mars also has been a frequent target of ground-based radars. In 1971 and 1973, an intense ranging campaign of the Mars equatorial regions led to topographic maps, which were the standard reference for many years [34]. Since then, every Mars landing mission, including Viking, Pathfinder, the Mars Exploration Rovers (MERs), and Phoenix, has used the ground-based radars to help winnow down the set of scientifically interesting landing sites by measurement of their surface roughness (e.g., [35]–[38]). Since Pathfinder and the MERs were dependent on a solid-surface-sensing radar for final descent, a key contribution of the Goldstone radar was in validating the radar reflectivity of the various sites in addition to the roughness determinations.

The Cassini mission to Saturn carried the European-built Huygens probe to land on Titan, the largest moon of Saturn. The Huygens probe descended into the thick atmosphere of Titan, which some scientists hypothesized was a by-product of an ocean of hydrocarbons that was kilometers deep. Joint observations by the Goldstone radar and the VLA determined that these fears were exaggerated, and that continent-sized regions of ice protruded through the ocean [39]. The Arecibo radar also observed Titan at 13 cm in 2001 and 2002, and obtained specular echoes consistent with reflection from areas of liquid hydrocarbons [40]. The radar on-board the Cassini spacecraft performed flyby radar imaging of Titan. After the Huygens Probe descent to Titan's surface, the Cassini radar determined that hydrocarbon (ethane mixed with methane) lakes could be found, but no very large seas, much less a ubiquitous kilometers-deep ocean.

In 1999, the Goldstone radar played an unusual role in support of the ESA/NASA SOHO mission, actually resulting in helping to save the spacecraft [41]. The SOHO solar observatory, in an L1-halo orbit near the Earth, accidentally used a large part of its attitude control thruster fuel, which left the spacecraft spinning at a rate that made telemetry contact useless. Ground-based radar observations in which Arecibo-transmitted and Goldstone-received CW radar

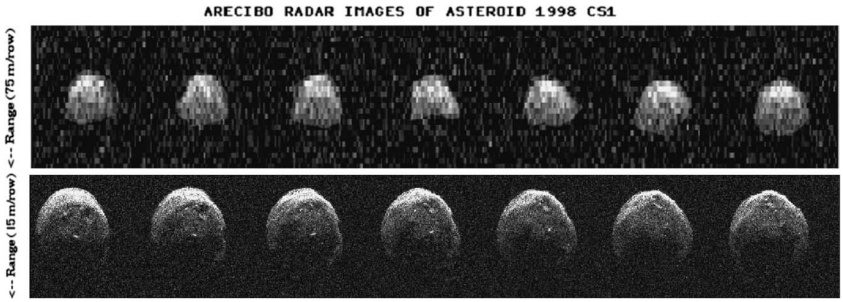

Fig. 12. ***The chirp ranging system increases the GSSR ranging resolution by a factor of five, from 18.75 to 3.75 m. This figure shows the significance of a factor of five improved resolution for NEO 1998 CS1 from 75 m per row at the top to 15 m per row at the bottom.***

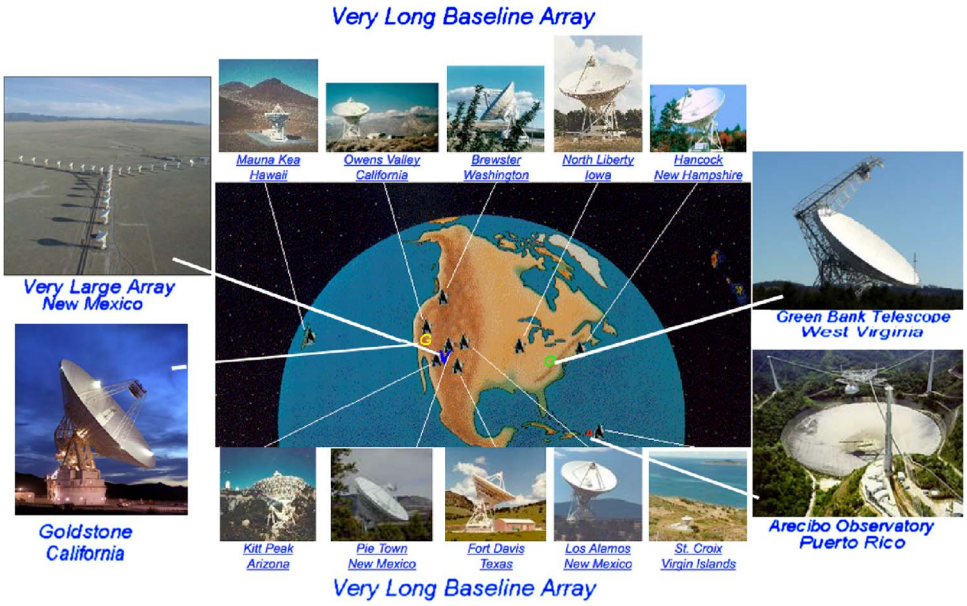

Fig. 13. ***The locations of the VLBA telescopes, the GBT, Arecibo, Goldstone, and the VLA within the United States.***

returns at S-band from SOHO determined the rate at which the SOHO spacecraft was spinning. Moreover, the radar echoes showed that the spin rate was low enough that a fraction of the remaining thruster propellant could bring SOHO back to rotating at a Sun-synchronous rate. As of 2010, SOHO (which cost about a billion Euros) was still operating.

One additional use of the Goldstone radar is its participation in a NASA program of monitoring orbital debris around the Earth. The Goldstone radar provides unique information on clouds of extremely small particles, ranging from about 1–10 mm, orbiting between altitudes of about 400–2500 km. [42]. Even particles of this small size, moving at extremely high velocities, can pose safety hazards to both human and robotic spacecraft. These radar observations continue to be important to astronauts moving on the exterior of the International Space Station.

VIII. FUTURE DIRECTIONS FOR THE GSSR

As mentioned above, the resolution of NEO imaging at the Goldstone radar could be improved to significantly finer than the current 3.75-m range resolution. Even though this is a factor of five higher than the previous best range resolution at Goldstone (see Fig. 12 for a pictorial version of what a factor of five can gain), this could be improved to about 1-m range resolution with no difficulty in principle. The fundamental limitation to the range resolution is the bandwidth of the klystron power amplifiers through which the "chirp" waveform passes. The spectrum allocation of the Goldstone radar is from 8500 to 8620 MHz (120-MHz

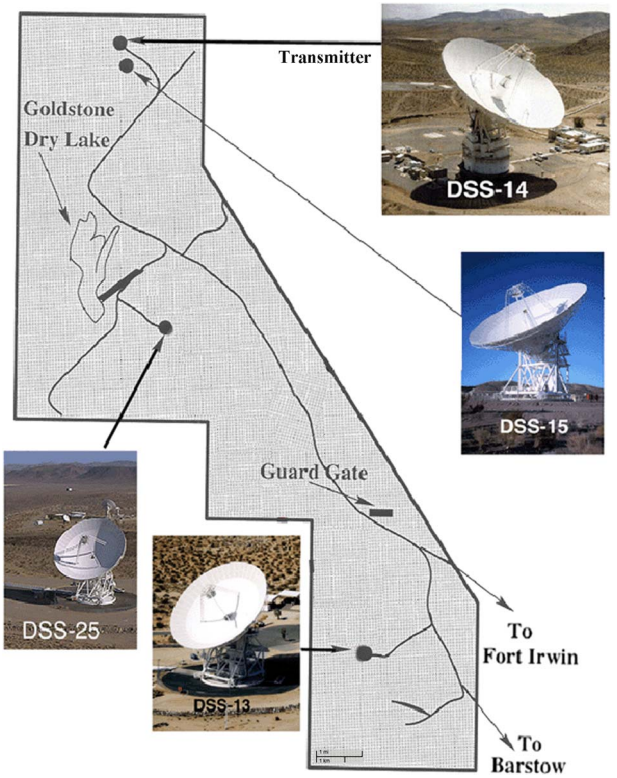

Fig. 14. ***The locations of radio telescopes at the Goldstone Deep Space Communications Complex (GDSCC). North is towards the top. The scale can be quickly understood from knowing that the baseline length between Deep Space Station (DSS)-25 and DSS-13 is 13 km. Three telescopes are nearly colocated at the "Apollo" complex: DSS-25, DSS-24, and DSS-26. All of these radio telescopes have been used as receivers by the GSSR.***

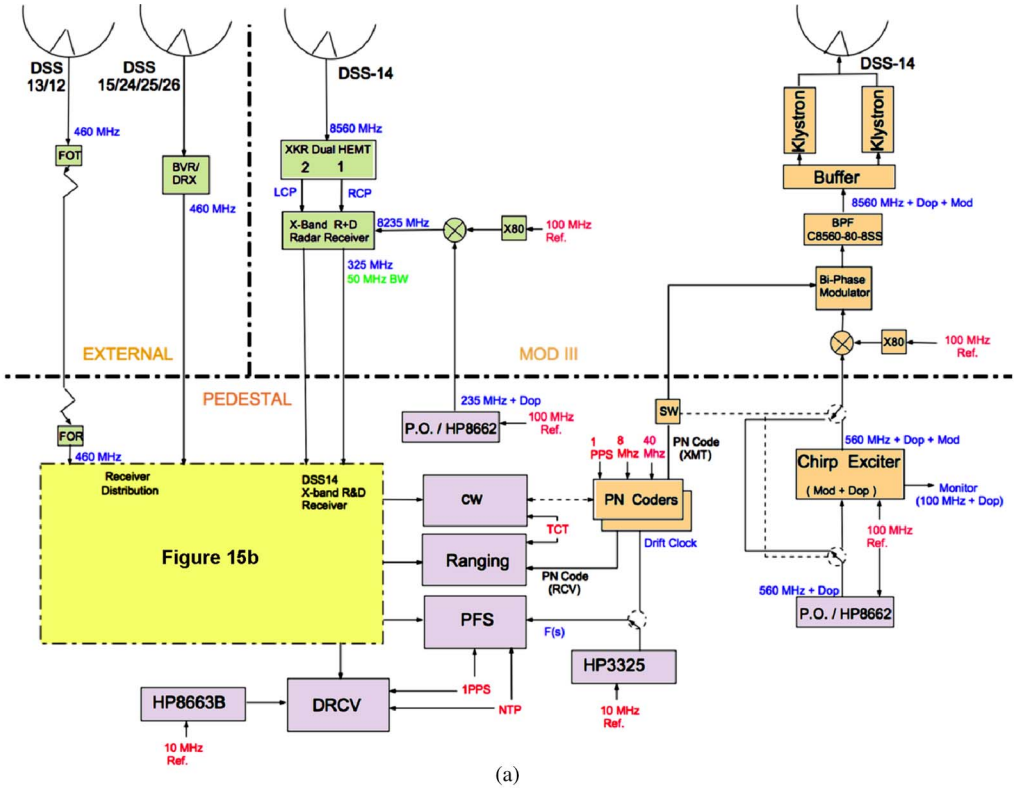

(a)

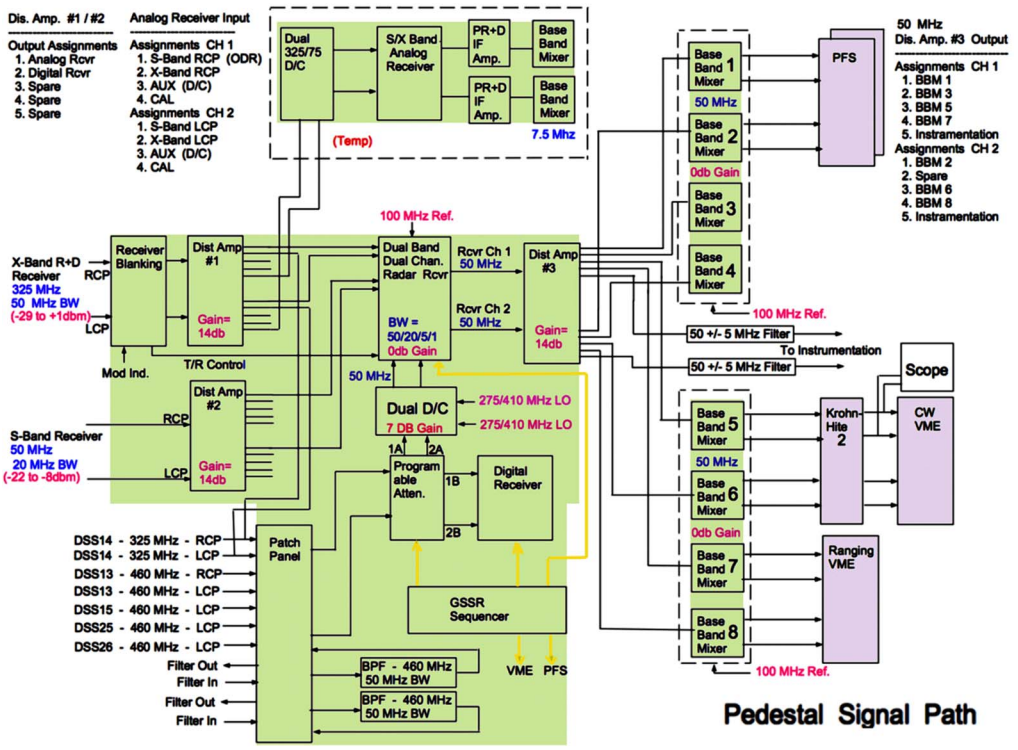

(b)

Fig. 15. *(a) A block diagram of the GSSR hardware in the DSS-14 pedestal (immediately below the azimuth bearing), the so-called MOD III area above the pedestal and below the elevation tracks. The colors are assigned as in Fig. 2. The area to the upper left shows telescopes elsewhere in the Goldstone complex. Acronyms: FOT = fiber optic transmitter; FOR = fiber optic receiver; BVR = block V Receiver (DSN hardware); DRCV = digital receiver (not shown is DRCV disk storage array); BPF = band pass filter; PFS = portable fast sampler; TCT = time code translator. (b) Continues from Fig. 15(a) as indicated there.*

bandwidth). The range resolution of the Goldstone radar could be improved most simply by procuring power amplifiers that would safely pass a broader bandwidth chirp than the 40-MHz bandwidth amplifiers currently in use. If power amplifiers could be obtained with 150-MHz of usable bandwidth, then 1-m range resolution could be achieved. However, to achieve 1-m resolution in cross range (Doppler shift), longer coherent integration times would be required. Only then could images with $(1\ \mathrm{m})^2$ pixel sizes be made.

Delay-Doppler radar NEO images with 3.75-m range resolution will lead to dramatic improvement in our knowledge of NEO sizes, shapes, and detailed surface structure. Finer details for NEO surfaces will facilitate much improved insight into NEO geology and collisional evolution. The detection of asteroid satellites will be significantly enhanced by the increase in resolution. For many NEOs, the higher resolution will permit much finer fractional precision Goldstone radar ranging astrometry than was previously possible, which will improve long-term orbital prediction for such objects.

IX. CONCLUSION

From the planet closest to the Sun to the icy moons of Jupiter and beyond to Saturn's rings and Titan, the Goldstone radar has performed extraordinarily valuable science and contributed to nearly every NASA solar system flight project, and is expected to continue doing so. The NASA investment in this radar observatory has resulted in significant enhancements (and frequently success-critical observations) for NASA's Flight Projects program, and has greatly benefited NASA's science investigations. ■

APPENDIX I
RADIO TELESCOPES IN THE UNITED STATES USED WITH THE GSSR

The telescopes to which the GSSR transmits (some shown in Fig. 13) must have extremely accurate frequency standards such as a cesium or a hydrogen maser "clock." Commercial cesium clocks have been available since the 1950s. Such "clocks" are essential for multistation radar astronomy. Synchronization to universal time "coordinated" (UTC) has been greatly simplified by the global positioning system (GPS), which can provide very accurate timing signals with accuracy of about 50 ns for observatories around the world. The Goldstone complex (Fig. 14) has frequency and timing signals distributed to all telescopes by buried fiber optical cable at sufficient depth to avoid daily heating effects changing the fiber propagation speed. See [43] for the factors that permit the Goldstone telescopes to operate as a very large connected-element interferometer.

APPENDIX II
DETAILED BLOCK DIAGRAMS FOR THE GSSR

A more complete explanation of the conceptual diagram of Fig. 2 is shown in Fig. 15. The "programmable oscillators" or POs of Figure 2 are further explained below. The PO is a frequency generator whose output signal is controlled by a "numerically controlled oscillator" (NCO). The NCO is, in turn, driven by an embedded computer, which changes the output frequency as given by reading an ephemeris file appropriate to the observation. The next generation PO (currently being integrated into the system) is a mixed-signal multilayer printed circuit board (PCB) which uses a field-programmable gate array (FPGA) in place of the embedded computer. The ephemeris information is loaded into the FPGA through a dynamic reconfiguration port. This port gives the ability to reconfigure only that portion of the FPGA that holds the polynomials for the ephemeris calculation, while leaving unchanged the portion of the device that implements the main PO function of calculating the frequency as a function of time.

Acknowledgment

The authors gratefully acknowledge the improvements made to this paper based on comments from reviewer Dr. L. Harcke and several anonymous reviewers.

REFERENCES

[1] S. J. Ostro, "Planetary radar," in *Encyclopedia of the Solar System*, L. A. McFadden, P. Weissman, and T. V. Johnson, Eds., 2nd ed. New York: Academic, 2007, pp. 735–764.

[2] R. M. Goldstein, R. R. Green, and H. C. Rumsey, "Venus radar brightness and altitude images," *Icarus*, vol. 36, no. 3, pp. 334–352, Aug. 1978.

[3] J. K. Harmon, "Planetary delay-Doppler radar and the long-code method," *IEEE Trans. Geosci. Remote Sens.*, vol. 40, no. 9, pp. 1904–1916, Sep. 2002.

[4] L. J. Harcke, "Radar imaging of solar system ices," Ph.D. dissertation, Dept. Elect. Eng., Stanford Univ., Stanford, CA, 2005.

[5] N. J. S. Stacy, "High-resolution synthetic aperture radar observations of the moon," Ph.D. dissertation, Dept. Astronomy, Cornell Univ., Pittsburgh, PA, 1993.

[6] J. L. H. Webb, D. C. Munson, and N. J. S. Stacy, "High-resolution planetary imaging via spotlight-mode synthetic aperture radar," *IEEE Trans. Image Process.*, vol. 7, no. 11, pp. 1571–1582, Nov. 1998.

[7] I. I. Shapiro, S. H. Zisk, A. E. E. Rogers, M. A. Slade, and T. W. Thompson, "Lunar topography: Global determination by radar," *Science*, vol. 178, no. 4064, pp. 939–948, Dec. 1972.

[8] S. H. Zisk, "A new, earth-based radar technique for the measurement of lunar topography," *The Moon*, vol. 4, no. 3/4, pp. 296–306, Sep. 1972.

[9] H. A. Zebker and R. M. Goldstein, "Topographic mapping from interferometric SAR observations," *J. Geophys. Res.*, vol. 91, no. B5, pp. 4993–4999, Apr. 1986.

[10] R. Gens and J. L. Van Genderen, "Review article: SAR interferometry-issues, techniques, applications," *Int. J. Remote Sens.*, vol. 17, pp. 1803–1835, 1996.

[11] J. L. Margot, D. B. Campbell, R. F. Jurgens, M. A. Slade, and N. J. Stacey, "Digital elevation models of the moon," *IEEE Trans.*

Geosci. Remote Sens., vol. 38, no. 2, pt. 2, pp. 1122–1133, Mar. 2000.

[12] S. Hensley, E. Gurrola, L. Harcke, M. Slade, K. Quirk, M. Srinivasan, C. Lee, S. Yun, J. Jao, B. Wilson, E. De Jong, N. Marechal, L. Weintraub, R. Dickinson, R. Bloom, G. Karamyan, and A. Lilje, "Lunar topographic mapping using a new high resolution mode for the GSSR radar," in *Proc. IEEE Nat. Radar Conf.*, Washington, DC, May 10–14, 2010, pp. 464–469.

[13] S. Hudson, "Three-dimensional reconstruction of asteroids from radar observations," *Remote Sens. Rev.*, vol. 8, pp. 195–203, Jul. 1993.

[14] C. Magri, S. J. Ostro, D. J. Scheeres, M. C. Nolan, J. D. Giorgini, L. A. M. Benner, and J.-L. Margot, "Radar observations and a physical model of asteroid 1580 Betulia," *Icarus*, vol. 186, pp. 152–177, Jan. 2007.

[15] C. Magri, *SHAPE Software Introduction and Documentation.* [Online]. Available e-mail: magri@maine.edu

[16] L. A. M. Benner, S. J. Ostro, M. C. Nolan, J.-L. Margot, J. D. Giorgini, R. S. Hudson, R. F. Jurgens, M. A. Slade, E. S. Howell, D. B. Campbell, and D. K. Yeomans, "Radar observations of asteroid 1999 JM8," *Meteoritics Planet. Sci.*, vol. 37, pp. 779–792, Jun. 2002.

[17] R. S. Hudson and S. J. Ostro, "Shape and non-principal axis spin state of asteroid 4179 Toutatis," *Science*, vol. 270, pp. 84–86, Oct. 1995.

[18] L. A. M. Benner, M. W. Busch, S. J. Ostro, J. D. Giorgini, A. A. Hine, J. K. Harmon, M. C. Nolan, R. Rose, R. F. Jurgens, J. S. Jao, C. Magri, and J.-L. Margot. (2006, Aug.). Radar images of asteroid 100085 (1992 UY4). presented at the IAU Symp. No. 236, Near-Earth Objects, Prague, Czech Republic. [Online]. Available: http://hdl.handle.net/2014/39808

[19] S. J. Ostro, R. F. Jurgens, K. D. Rosema, R. S. Hudson, J. D. Giorgini, R. Winkler, D. K. Yeomans, D. Choate, R. Rose, M. A. Slade, S. D. Howard, D. J. Scheeres, and D. L. Mitchell, "Radar observations of asteroid 1620 geographos," *Icarus*, vol. 121, pp. 46–66, May 1996.

[20] S. J. Ostro, R. S. Hudson, R. F. Jurgens, K. D. Rosema, R. Winkler, D. Howard, R. Rose, M. A. Slade, D. K. Yeomans, J. D. Giorgini, D. B. Campbell, P. Perillat, J. F. Chandler, and I. I. Shapiro, "Radar images of asteroid 4179 Toutatis," *Science*, vol. 270, pp. 80–84, Oct. 1995.

[21] R. S. Hudson, S. J. Ostro, and D. J. Scheeres, "High-resolution model of asteroid 4179 Toutatis," *Icarus*, vol. 161, pp. 346–355, Feb. 2003.

[22] D. K. Yeomans, S. J. Ostro, and P. W. Chodas, "Radar astrometry of near-Earth asteroids," *Astron. J.*, vol. 94, pp. 189–200, Jul. 1987.

[23] S. J. Ostro, J. L. Margot, L. A. M. Benner, J. D. Giorgini, D. J. Scheeres, E. G. Fahnestock, S. B. Broschart, J. Bellerose, M. C. Nolan, C. Magri, P. Pravec, P. Scheirich, R. Rose, R. F. Jurgens, E. M. de Jong, and S. Suzuki, "Radar imaging of binary near-earth asteroid (66391) 1999 KW4," *Science*, vol. 314, pp. 1276–1280, Nov. 2006.

[24] C. E. Cook and M. Bernfeld, *Radar Signals,* 1st ed. New York: Academic, 1967.

[25] C. Elachi, *Introduction to the Physics and Techniques of Remote Sensing,* 1st ed. New York: Wiley, 1987ISBN: 0471848107.

[26] J. L. Margot, *Planetary, Radar Astronomy With Linear FM (Chirp) Waveforms*, Internal Arecibo Memo, Jun. 2000.

[27] K. Quirk and M. Srinivasan, *GSSR Waveforms for Lunar Observations*, Internal JPL Study, Mar. 2008.

[28] NASA. (2010). *Near Earth Object Program.* [Online]. Available: http://neo.jpl.nasa.gov/news/news167.html

[29] G. Chin, S. Brylow, M. Foote, J. Garvin, J. Kasper, J. Keller, M. Litvak, I. Mitrofanov, D. Paige, K. Raney, M. Robinson, A. Sanin, D. Smith, H. Spence, P. Spudis, S. A. Stern, and M. Zuber, "Lunar reconnaissance orbiter overview: The instrument suite and mission," *Space Sci. Rev.*, vol. 129, no. 4, pp. 391–419, Apr. 2007.

[30] I. V. Kholin, "Accuracy of body-rotation-parameter measurement with monochromatic illumination and two-element reception," *Radiophys. Quantum Electron.*, vol. 35, pp. 284–287, May 1992.

[31] J. L. Margot, S. J. Peale, R. F. Jurgens, M. A. Slade, and I. V. Holin, "Large longitude libration of Mercury reveals a molten core," *Science*, vol. 316, pp. 710–714, May 2007.

[32] M. A. Slade, S. Zohar, and R. F. Jurgens, "Venus: Improved spin vector from Goldstone radar observations," *Astronom. J.*, vol. 100, pp. 1369–1374, Oct. 1990, (plates 1396–1401).

[33] I. I. Shapiro, J. F. Chandler, D. B. Campbell, A. A. Hine, and N. J. S. Stacy, "The spin vector of Venus," *Astronom. J.*, vol. 100, pp. 1363–1368, Oct. 1990.

[34] G. S. Downs, P. E. Reichley, and R. R. Green, "Radar measurements of Martian topography and surface properties: The 1971 and 1973 oppositions," *Icarus*, vol. 26, pp. 273–312, Nov. 1975.

[35] G. L. Tyler, D. B. Campbell, G. S. Downs, R. R. Green, and H. J. Moore, "Radar characteristics of Viking 1 landing sites," *Science*, vol. 193, pp. 812–815, Aug. 1976.

[36] A. F. C. Haldemann, D. L. Mitchell, R. F. Jurgens, M. A. Slade, and D. O. Muhleman, "Mars pathfinder landing site assessment with Goldstone delay-Doppler and CW-radar experiments," *J. Geophys. Res. Planets*, vol. 102, no. E2, pp. 4097–4106, Feb. 1997.

[37] M. P. Golombek, J. A. Grant, T. J. Parker, D. M. Kass, J. A. Crisp, S. W. Squyres, A. F. C. Haldemann, M. Adler, W. J. Lee, N. T. Bridges, R. E. Arvidson, M. H. Carr, R. L. Kirk, P. C. Knocke, R. B. Roncoli, C. M. Weitz, J. T. Schofield, R. W. Zurek, P. R. Christensen, R. L. Fergason, F. S. Anderson, and J. W. Rice, Jr., "Selection of the Mars Exploration Rover landing sites," *J. Geophys. Res.*, vol. 108, pp. 13–33, Dec. 2003.

[38] A. F. C. Haldemann and B. J. Butler, "Evaluation of the Phoenix Region B landing site rock coverage from available radar data," in *Proc. 4th Int. Conf. Mars Polar Sci. Explorat.*, Oct. 2006, p. 8057, LPI Contribution No. 1323.

[39] D. O. Muhleman, A. W. Grossman, B. J. Butler, and M. A. Slade, "Radar reflectivity of Titan," *Science*, vol. 248, pp. 975–980, May 1990.

[40] D. B. Campbell, G. J. Black, L. M. Carter, and S. J. Ostro, "Radar evidence for liquid surfaces on Titan," *Science*, vol. 302, no. 5644, pp. 431–434, Oct. 2003.

[41] F. C. Vandenbussche. (1999, Mar.). *SOHO's Recovery—An Unprecedented Success,* ESA, Noordwijk, The Netherlands. [Online]. Available: http://www.esa.int/esapub/bulletin/bullet97/vandenbu.pdf

[42] R. M. Goldstein, S. J. Goldstein, and D. J. Kessler, "Radar observations of space debris," *Planetary Space Sci.*, vol. 46, pp. 1007–1013, Aug. 1998.

[43] J. Lauf, M. Calhoun, W. Diener, J. Gonzalez, A. Kirk, P. Kuhnle, B. Tucker, C. Kirby, and R. Tjoelker. (2005, Aug.). *Clocks and Timing in the NASA Deep Space Network,* Jet Propulsion Laboratory, Pasadena, CA. [Online]. Available: http://www.dtic.mil/cgibin/GetTRDoc?Location=U2&doc=GetTRDoc.pdf&AD=ADA483368

ABOUT THE AUTHORS

Martin A. Slade (Member, IEEE) received the B.S. and M.S. degrees in physics and the Ph.D. degree in earth, atmospheric, and planetary science from the Massachusetts Institute of Technology, Cambridge in 1964, 1967, and 1971 respectively.

Currently, he is a Group Supervisor of the Solar System Radar Group at the Jet Propulsion Laboratory (JPL), California Institute of Technology, Pasadena. His scientific interests have ranged from testing of gravitational theories that generalize "metric" theories (such as general relativity) to very long baseline observations of the structure of quasars and active galactic nuclei. Currently, the determinations of time variations in the spin vector and rotation period for both Mercury and Venus are ongoing collaborative research areas in radar astronomy. Other scientific interests are radar mapping of the topography of the lunar poles and the surface of Mercury. The determination by radar of the shapes, orbits, and physical characterization for near-Earth asteroids and comets is an active area of collaboration with scientists at JPL and elsewhere.

Dr. Slade is a member of the American Geophysical Union, the American Astronomical Society (Division for Planetary Sciences and Division on Dynamical Astronomy), and the International Astronomical Union.

Lance A. M. Benner received the A.B. degree in physics from Cornell University, Ithaca, NY, in 1987 and the Ph.D. degree in earth and planetary science from Washington University in St. Louis, St. Louis, MO, in 1994.

Currently, he is a Research Scientist at the Jet Propulsion Laboratory, California Institute of Technology, Pasadena. He has served in this position since 2003. Prior to that, he was a Scientist from 1998, and a National Research Council Postdoctoral Fellow from 1995. Both of these positions were at the JPL. Prior to work at JPL, he was a Postdoctoral Research Associate, Washington University, Seattle, from 1994. He has authored more than 50 papers on asteroids and comets. He specializes in radar imaging of near-Earth and main-belt asteroids using the NSF's Arecibo Observatory (Puerto Rico) and NASA's Goldstone Solar System Radar (California), and he has participated in radar observations of more than 200 near-Earth asteroids.

Dr. Benner is a member of the American Astronomical Society (Division for Planetary Sciences), the Meteoritical Society, the American Geophysical Union, and the International Meteor Organization.

Arnold Silva received the B.S. degree from the California State University at Los Angeles, Los Angeles, in 1981 and the M.S. degree from the California State University at Northridge, Northridge, in 1987, both in electrical engineering, with emphasis on power, communications, and radar.

In 1981, he joined the Transmitter Group of ITT Gilfillan and was involved in the design of high-power modulators, power converters, and control circuits for the company's major radar programs. From 1989 to 1993, he was employed as an Engineering Specialist of Whittaker Electronic Systems engaged in the design, simulation, and analysis of radar transmitter systems and subsystems, for both classified and unclassified programs. His designs involved development of very high-power, low phase noise transmitters (pulsed and CW). In 1993, he joined the Jet Propulsion Laboratory, California Institute of Technology, Pasadena, as a Member of the Technical Staff in the Transmitter Engineering Group. In October 2010, he became a Senior Project Leader at The Aerospace Corporation, El Segundo, CA. He has designed ultra phase and amplitude stable high-voltage power subsystems and RF subsystems for the S-band and X-band Deep Space Network (DSN) klystron-based transmitter uplinks. These systems ranged in power up to 500 KW CW radiated. In 1998, he assumed the position of Group Supervisor for the Transmitter Engineering Group. In 2010, he assumed the role of System Engineer for overall DSN Facilities, Power, and Infrastructure.